NONSTATIONARY PLANE WAVES IN MEDIA WITH BULK VISCOSITY

G. M. Lyakhov and V. N. Okhitin

UDC 624.131+532.529

The propagation of plane waves in media endowed with bulk viscosity and characterized by linear dynamic and static compression p—V diagrams has been investigated earlier [1-3]. For a large pressure differential it is necessary to take account of the nonlinearity of these diagrams, and in the case of spherical waves in solids it is also necessary to include the plasticity condition. The Mises—Schleicher plasticity condition has been proposed for soils and rocks [4]. Spherical detonation waves have been analyzed for a nonlinear compression p—V diagram in multicomponent media (water-impregnated soils, water containing gas bubbles, etc.) without regard for viscosity [5], and the same has been done for plane waves with allowance for viscosity, but in the case of steady shock loading [6].

In the present article we use the method of characteristics to solve the problem of propagation of a plane wave generated by nonsteady shock loading in a medium with bulk viscosity for nonlinear dynamic (impact) and static (corresponding to the equilibrium state) compression p—V diagrams. We use a special model of a multicomponent medium [3] to perform computer calculations. We carry out simultaneous calculations for the same medium without viscosity and with a p—V diagram corresponding to static compression.

We use other models as well [7-14] to investigate waves in viscous media. Godunov and Kozin's equation for the medium [7] include viscoelastic terms corresponding to the Maxwell model. Babe and others [8] introduce a viscosity term in the Mises—Schleicher plasticity condition. Koshelev's medium [9] obeys the Kelvin—Voigt model in the uniaxial stressed state and is not compressed in the complex stressed state, the plasticity condition depending on the strain rate. Zubkova and Rykov [10] recommend the Mises—Schleicher plasticity condition to account for the influence of strain rate on compressibility. Ting [11] uses the Maxwell model with a temperature-dependent viscosity coefficient. According to Akoi and Hori [12], a viscoelastic relation exists between the stress and strain deviators. Jong and others [13] apply the Kelvin—Voigt model to soils. Zabinski and Phillips [14] find that the medium is elastic in hydrostatic compression and has viscous properties in shear loading.

§1. The following notation is used in our model [3] for a three-component medium. At atmospheric pressure p_0 (α_1, α_2 and α_3 are the volumetric contents of the gaseous, liquid, and solid components; V_{10}, V_{20}, and V_{30} are their specific volumes, respectively, ρ_{10}, ρ_{20}, ρ_{30} are the densities; c_{10}, c_{20}, c_{30} are the sound velocities in them; ρ_0 is the density of the medium; and V_0 is its specific volume) and at pressure p (the corresponding specific volumes, densities, and velocities are V_1, V_2, V_3, ρ_1, ρ_2, ρ_3, c_1, c_2, and c_3, respectively; the density of the medium is ρ; and its specific volume is V) we have the relations

$$\rho_0 = \alpha_1\rho_{10} + \alpha_2\rho_{20} + \alpha_3\rho_{30}, \quad \alpha_1 + \alpha_2 + \alpha_3 = 1.$$

The following equations are postulated for all components in the free state:

$$p = p_0 + \frac{\rho_{i0}c_{i0}^2}{\gamma_i}\left[\left(\frac{V_{i0}}{V_i}\right)^{\gamma_i} - 1\right], \tag{1.1}$$

where i is the component identification number.

Equation (1.1) corresponds to the Poisson adiabat for the gas and to the Tate equation for the other components. The gas exists in bubble form in the medium. The compression of the bubbles, which are isolated by the other components, takes place under loading in a finite time due to the displacement of the other components and filling of the bubble interiors with those components. We assume, therefore, that the compression of the gas in the bubbles (in the medium) obeys the law

Moscow. Translated from Zhurnal Prikladnoi Mekhaniki i Tekhnicheskoi Fiziki, No. 5, pp. 126-135, September-October, 1977. Original article submitted August 16, 1976.

0021-8944/77/1805-0693$07.50

TABLE 1

α_1	α_2	α_3	$A \cdot 10^{-6}$ kg·sec^{-1}·m^{-2}	$\eta \cdot 10^{-3}$ kg·sec^{-1}·m^{-1}	Medium
0,01	0,39	0,6	3,28	1,09	Water-impregnated soil
0,02	0,38	0,6	3,34	1,11	"
0,04	0,36	0,6	3,39	1,13	"
0,01	0,99	—	1,52	0,51	Water with gas bubbles
0,04	0,96	—	1,53	0,52	"
0,10	0,90	—	1,58	0,53	"

$$p = p_0 + \frac{\rho_{10} c_{10}^2}{\gamma_1}\left[\left(\frac{V_{10}}{V_1}\right)^{\gamma_1} - 1\right] - \eta\frac{\dot{V}_1}{V_{10}}$$

(η is the bulk viscosity coefficient of the medium). The other components are compressed as in the free state.

The compressibility equation for the three-component medium under these assumptions has the form [3]

$$\dot{V}/V_0 = \varphi(p)\dot{p} - \alpha_1\psi(p, V)/\eta, \tag{1.2}$$

where

$$\varphi(p) = -\sum_{i=2}^{3}\frac{\alpha_i}{\rho_{i0}c_{i0}^2}\left[\frac{\gamma_i(p-p_0)}{\rho_{i0}c_{i0}^2} + 1\right]^{-(1+\gamma_i)/\gamma_i}; \quad \psi(p, V) = p - p_0\alpha_1^{\gamma_1}\left\{\frac{V}{V_0} - \sum_{i=2}^{3}\alpha_i\left[\frac{\gamma_i(p-p_0)}{\rho_{i0}c_{i0}^2} + 1\right]^{-\gamma_i}\right\}^{-\gamma_1}.$$

The dynamic compressibility equation ($\dot{V} \to \infty$, $\dot{p} \to \infty$) is

$$\frac{V_D}{V_0} = \alpha_1 + \sum_{i=2}^{3}\alpha_i\left[\frac{\gamma_i(p-p_0)}{\rho_{i0}c_{i0}^2} + 1\right]^{-1/\gamma_i}, \quad \varphi(p) = \rho_0\frac{dV_D}{dp}. \tag{1.3}$$

The static compressibility equation ($\dot{V} \to 0$, $\dot{p} \to 0$) is

$$\frac{V_S}{V_0} = \sum_{i=2}^{3}\alpha_i\left[\frac{\gamma_i(p-p_0)}{\rho_{i0}c_{i0}^2} + 1\right]^{-1/\gamma_i}. \tag{1.4}$$

The dynamic compressibility of water containing gas bubbles corresponds to the compressibility of water, whereas for water-impregnated soil it corresponds to the compressibility of a two-component medium consisting of solid and liquid components. The gas is incompressible in shock compression of the medium. The static p–V diagram corresponds to the equilibrium state, where all components are compressed to the appropriate limit for the acting pressure [according to Eqs. (1.1)].

We use Lagrange variables: the spatial coordinate r and the time t.

In the initial cross section r = 0 at time t = 0, the pressure jumps instantly from p_0 to p and then varies according to the law

$$p = p_0 + p_m e^{-t/\theta}. \tag{1.5}$$

We propose to determine the parameters of the wave generated in the medium by this load.

The fundamental equations of motion are

$$\frac{\partial u}{\partial r} - \rho_0\frac{\partial V}{\partial t} = 0, \quad \frac{\partial u}{\partial t} + \frac{1}{\rho_0}\frac{\partial p}{\partial r} = 0. \tag{1.6}$$

The solution is reduced to integration of the system (1.6) closed by Eq. (1.2) and subject to the boundary conditions (1.5) in the initial cross section and, at the discontinuity (precursor),

$$p - p_0 = \rho_0 uD, \quad (\rho - \rho_0)D = \rho u.$$

To determine the influence of the bulk viscosity on the wave parameters we solve the same problem for the medium without viscosity, characterized by a compressibility and unloading equation coinciding with the static compressibility equation (1.4) for the viscous medium.

We transform to dimensionless variables and dimensionless Lagrange variables

$$p^0 = p/p_0, \quad V^0 = V/V_0, \quad u^0 = u/c_n, \quad D^0 = D/c_n, \quad x^0 = Ar/3\eta, \quad t^0 = Ac_n t/3\eta.$$

In these variables the fundamental equations are

$$\frac{\partial u^0}{\partial x^0} - \frac{\partial V^0}{\partial t^0} = 0, \quad \frac{\partial u^0}{\partial t^0} + \frac{p_0}{\rho_0 c_n^2}\frac{\partial p^0}{\partial x^0} = 0;$$

the loading in the initial cross section is

$$p^0 = 1 + p_m^0 e^{-\eta t^0},$$
$$\theta^0 = Ac_n\theta/3\eta = \lambda\theta, \quad \lambda = Ac_n/3\eta;$$

the equation describing the behavior of the medium is

$$\frac{\partial V^0}{\partial t^0} = \varphi^0(p^0)\frac{\partial p^0}{\partial t^0} - \alpha_1\psi^0(p^0, V^0),$$

$$\varphi^0(p^0) = -\sum_{i=2}^{3}\frac{\alpha_i p_0}{\rho_{i0}c_{i0}^2}\left[\frac{\gamma_i(p^0-1)p_0}{\rho_{i0}c_{i0}^2}+1\right]^{-\frac{1+\gamma_i}{\gamma_i}},$$

$$\psi^0(p^0, V^0) = \frac{3p_1}{Ac_n}\left[p^0 - \alpha_1^{\gamma_1}\left\{V^0 - \sum_{i=2}^{3}\left[\frac{\gamma_i(p^0-1)p_0}{\rho_{i0}c_{i0}^2}+1\right]^{-1/\gamma_i}\right\}^{\gamma_1}\right],$$

$$A = \left(\frac{\alpha_2\rho_{20}+\alpha_3\rho_{30}}{1-\alpha_1}\right)^{1/2}\left(\frac{\alpha_2}{\rho_{20}c_{20}^2}+\frac{\alpha_3}{\rho_{30}c_{30}^2}\right)^{-1/2}$$

(A is the acoustic impedance of the two-component medium surrounding the gas bubbles). The viscosity coefficient η is determined experimentally. Approximate values of η can be obtained from the equation [3]

$$\eta = Ar_0/3.$$

The calculated values of η for gas bubbles of radius $r_0 = 10^{-3}$ m are given in Table 1. In this case the dimensionless variables take the form

$$x^0 = r/r_0, \quad t^0 = c_n t/r_0, \quad \theta^0 = c_n\theta/r_0.$$

In the new variables, the problem involves one less parameter than in the old variables. The solution is determined by the product $\lambda\theta$. This fact permits the results of a single calculation to be applied to several media (with different values of η) or loads (with different values of θ).

The dimensionless equation describing the behavior of the nonviscous media, according to (1.4), has the form

$$V^0 = \sum_{i=1}^{3}\alpha_i\left[\frac{\gamma_i(p^0-1)p_0}{\rho_{i0}c_{i0}^2}+1\right]^{-1/\gamma_i}.$$

We have solved the problem on a computer by the method of characteristics, which has been applied earlier to nonviscous media [15, 5] and to bulk-viscous media [3, 6]. For the calculations we used the parameters $\rho_{10} = 1.29$ kg/m^3, $\rho_{20} = 10^3$ kg/m^3, $\rho_{30} = 2.65 \cdot 10^3$ kg/m^3, $c_{10} = 330$ m/sec, $c_{20} = 1500$ m/sec, $c_{30} = 4500$ m/sec, $\gamma_1 = 1.4$, $\gamma_2 = 7$, $\gamma_3 = 4$, $c_n = 4250$ m/sec.

§2. The calculations show that an elastic shock (precursor) begins to propagate from the initial cross section in the viscous medium at the instant of application of impact loading. At short distances the post-shock pressure decreases, at fairly large distances it continues to increase and then decrease, and at still greater distances the magnitude of the shock is almost equal to zero, the disturbance degenerating into a continuous compression wave.

We now discuss the results of calculations of the pressure, particle velocity, and volume in a three-component medium (water-impregnated soil) with $\alpha_1 = 0.01$, $\alpha_2 = 0.39$, $\alpha_3 = 0.6$ under loading with $p^0 = 50$ and $\theta^0 = 5000$. Figure 1 gives the diagrams $V_D^0(p^0)$ and $V_S^0(p^0)$ in dynamic and static compression of this medium, calculated according to (1.3) and (1.4). Curves 0-5 represent the variations of the state of particles of the medium at distances $x^0 = 0$, 20, 100, 500, 1000, and 2000, respectively. In the course of wave propagation at each distance, after the precursor shock originating along the dynamic diagram, the state of the particles gradually approaches the static diagram and crosses over into the region of smaller volumes. As the wave moves farther along, smearing causes the compression and loading regime to approach

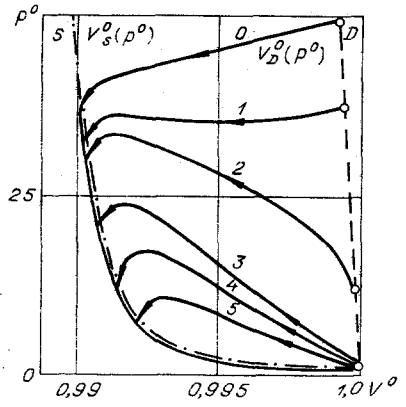

Fig. 1

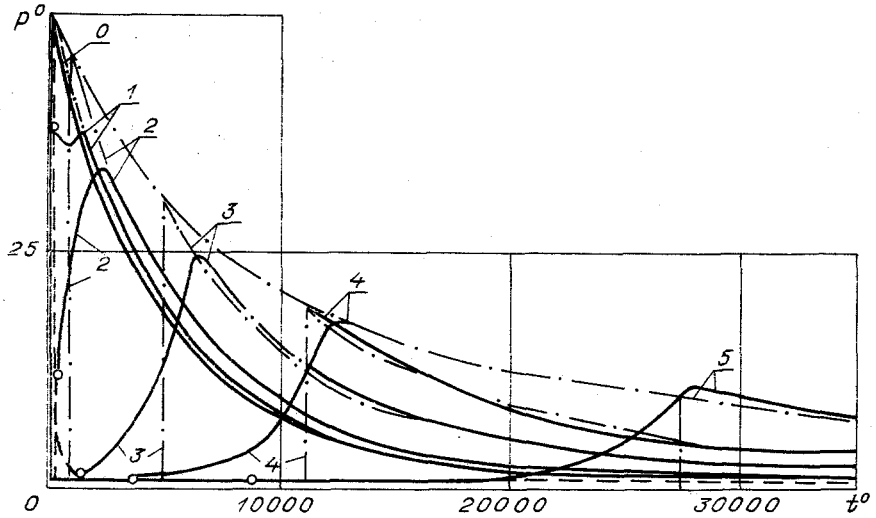

Fig. 2

the static regime. The minimum volume is attained, not at the pressure maximum, but during the period of its decline.

Figure 2 gives the time variation of the pressure at fixed particles. Curves 0-5 refer to particles with coordinates x^0 = 0, 20, 100, 500, 1000, and 2000, respectively. The solid curves represent the pressure in the viscous medium and the dashed-dot curves correspond to the pressure in the nonviscous medium.

Close to the initial cross section in the viscous medium, the wave represents a shock. The magnitude of the shock decreases with distance, and for $x^0 \geq 500$ it is practically equal to zero. For $x^0 \leq 20$ the pressure in the viscous medium has two maxima, and at large distances it has just one maximum. In the latter case a continuous growth, and then a decrease, of the pressure takes place behind the shock. The presence of two maxima close to the point of application of the load has been noted in a medium with linear dynamic and static compression p—V diagrams [16]. The magnitudes of the shocks are indicated by circles.

The precursor velocity is determined by the dynamic compression diagrams and, due to the nonlinearity of the diagram, decreases with distance. The velocity of propagation of the pressure maximum is less than the precursor velocity. It increases with distance at first, then decreases,and comes close to the wave velocity in the nonviscous medium, but it can attain even smaller values.

The pressure maximum is overtaken by the shock in the nonviscous medium, and near the initial cross section it is greater than in the viscous medium. With increasing distance the values of the maxima for both media approach one another. The pressure in the nonviscous medium can become less than in the viscous medium. The difference between the maximum pressures with and without viscosity taken into account is small, not more than a few percent. The decay of the pressure at the particles with time near the initial cross section differs in the two cases, but with greater distance it is practically the same. The bulk viscosity causes the wave to smear, altering its profile mainly in the pressure growth period.

Figure 3 gives the time variation of the particle velocities u^0 at distances x^0 = 0, 500, 1000, and 2000 (curves 0, 3-5, respectively). The curves have the same numbering scheme as in Fig. 2. At all distances in the viscous medium, the velocity grows continuously after the shock. With increasing distance the shock tends to zero, and the time at which the maximum is attained increases. The velocity attains its maximum in the period of declining pressure. The maximum particle at all distances in the viscous medium is smaller than in the nonviscous medium.

Figure 4 gives the time variation of the volume for x = 0, 500, 1000, and 2000 (curves 0, 3-5, respectively). In the viscous medium, the volume drops abruptly (at the precursor), continues to decrease to a minimum, and then increases to the initial value. The magnitude of the volume drop decreases to zero with distance. The volume changes abruptly in the nonviscous medium, and its external value is several percent greater than in the viscous medium.

The curves in Fig. 5 illustrate the dependence of the maximum pressure in the wave on the distance in the same three-component viscous medium under a load p^0 = 50, but for differ-

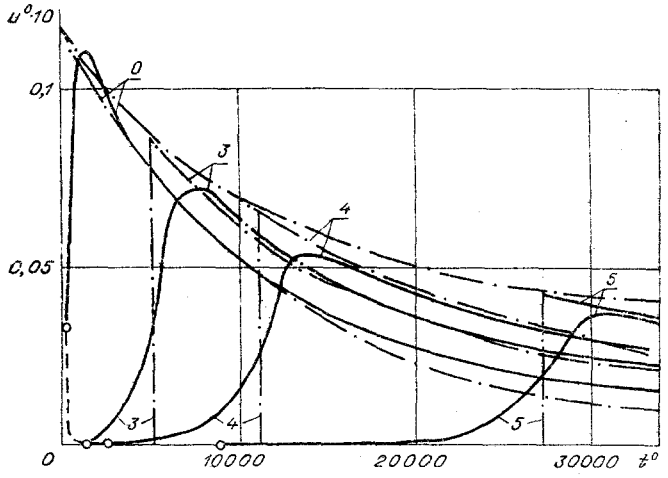

Fig. 3

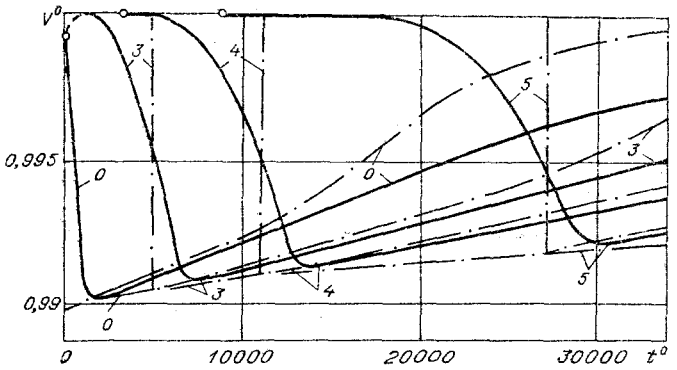

Fig. 4

ent values of θ°. For a constant viscosity coefficient, this situation is equivalent to different values of θ. Curves 1-3 correspond to values of $\theta^\circ = \infty$ (steady load), 5000, and 500, respectively, and curve 0 corresponds to the pressure at the precursor. In the region where the wave is a shock, the maximum pressure is attained at the precursor. For $\theta^\circ = \infty$ curves 1 and 0 originate from a common point. The precursor pressure does not depend on the value of θ°. With a decrease in θ° the decay rate of the maximum pressure with distance increases. Figure 5 also gives the paths of the precursor and pressure maximum. The velocity D° of propagation of the maximum at all distances decreases with the value of θ°. With increasing distance from the initial cross section D° increases at first, and then decreases. For $\theta^\circ = \infty$ the velocity becomes constant after the growth and decay period. For finite values of θ° the velocity decreases with distance to a value corresponding to the velocity of sound calculated according to the static diagram for $p^\circ \to 1$. For $p^\circ = 50$ and $\theta^\circ = \infty$, 5000, and 500, the maximum values of D° are approximately 0.14, 0.12, and 0.08, respectively. The maximum D° for $\theta^\circ = 500$ is attained at a distance $x^\circ \approx 100$. The maximum values of D° diminish appreciably as the value of θ° is decreased. The maximum precursor velocity in this case attains a value roughly equal to 0.4.

It follows from the calculations carried out for identical loads in the initial cross section and different proportions of the gaseous component in the medium that the rate of decay of the wave with distance increases with the value of α_1, consistent with experiment [3]. An increase of α_1 is equivalent to an increase of the difference between the dynamic and static p—V diagrams, which increases the energy losses associated with wave propagation.

The dependence $p^\circ(t^\circ)$ for a viscous medium with $\alpha_1 = 0.01$, $\alpha_2 = 0.39$, and $\alpha_3 = 0.6$ is plotted in Fig. 6 for $p^\circ = 10^4$ and $\theta^\circ = 100$. The maximum load in the initial cross section is 200 times greater, and the time θ° smaller by 1/50, than in the case of a wave having the profile in Fig. 2. Curves 0-6 refer to distances $x^\circ = 0.5 \cdot 10^3$, 10^4, $2 \cdot 10^4$, $3 \cdot 10^4$, $4 \cdot 10^4$, and $5 \cdot 10^4$, respectively. At a distance $5 \cdot 10^4$ the maximum pressure is less by about one-tenth than in the initial cross section. The pressure rise time to the maximum is approximately 230, i.e., greater than θ°. In Fig. 2 the pressure has decreased by about 1/5 at a

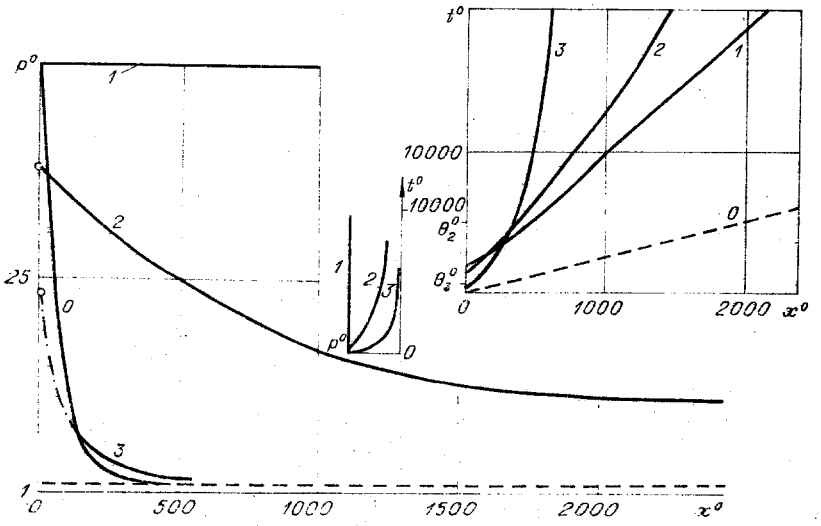

Fig. 5

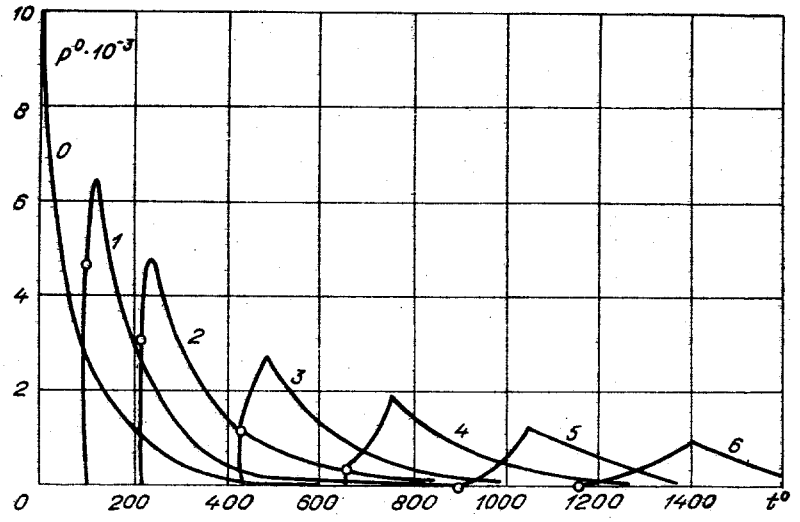

Fig. 6

distance of $2 \cdot 10^3$, and the rise time is greater than 10,000, i.e., very much greater than θ°. The wave profile changes considerably in both cases.

The values calculated for the maximum pressure with allowance for viscosity in water-impregnated solid and in water containing gas bubbles with identical proportions of the gaseous component $\alpha_1 = 0.01$, for a pressure $p^\circ = 50$ and time $\theta^\circ = 5000$, are given in Table 2. In water the pressure falls off more slowly with the distance x° than in water-impregnated soil.

Thus, bulk viscosity of a medium with nonlinear limiting compression p—V diagrams causes shock smearing, as was found earlier for the case of linear p—V diagrams [1, 3]. A precursor goes first, its velocity decreasing with distance in correspondence with the dynamic diagram, until it attains the velocity of sound. The magnitude of the precursor shock tends to zero in this case. The velocity of propagation of the pressure maximum increases at first with distance, and then decreases, gradually approaching the value determined by the static p—V diagram. In the limit, the velocity of the maximum decreases to the velocity of sound calculated from the static diagram. The maximum pressure tends to zero in this case.

The external values of the pressure, volume, and particle velocity, calculated with and without viscosity, are close to one another, the differences amounting to just a few percent. This result shows that the extremal values of the parameters can be estimated at large enough distances from the point of application of the load without concern for the viscosity, using the static diagram. On the other hand, the wave profile differs considerably according to whether viscosity is ignored or not. The wave profile, pressure rise time to the maximum,

TABLE 2

x^0	250	500	1000	1500	2000	Medium
p^0	34	29	21	15	13	Water with gas bubbles
p^0	28	24	17	13	9	Water-impregnated soil

and delay time of the particle velocity and volume relative to the pressure can be calculated only according to the model with viscosity. Waves with identical maximum pressure but different rise times to the maximum create different loads. This fact must be taken into account in deciding on the model for solution of a particular problem. We also point out that the investigated media are characterized by a relatively small difference between the dynamic and static compression p—V diagrams and by a bulk viscosity coefficient such as ensures rapid transition of the state of the medium from the dynamic to the static regime. The possibility of calculating the extremal values from the static diagram applies to such media.

The bulk viscosity is a property common to dense media: soils, rocks, metals, plastics, etc. Its quantitative manifestation is determined by the extent of the difference between the dynamic and static p—V diagrams, as well as by the value of the viscosity coefficient. In low-porosity rocks and metals, the differences between the limiting diagrams are small, and the state of the medium proceeds rapidly to the static diagram. In this case, as for water-impregnated soil, the allowance for bulk viscosity results in wave smearing, and the extremal values of the parameters vary only slightly, so that they can be calculated approximately from the static diagram. In highly porous rocks and in nonimpregnated soils, the differences between the limiting diagrams are large. Now the bulk viscosity leads to more pronounced wave smearing and variation of the extremal values of the parameters [3]. The general laws describing the deformation of dense media under dynamic loading depend significantly on the bulk viscosity and cannot be formulated solely on the basis of one of the limiting p—V diagrams in compression and unloading.

LITERATURE CITED

1. G. M. Lyakhov and I. T. Tropin, "Plane waves in soils and rocks as viscoelastic media," Izv. Akad. Nauk SSSR, Mekh. Tverd. Tela, No. 3 (1973).
2. G. M. Lyakhov and Ya. A. Pachepskii, "Allowance for viscous and plastic properties in the solution of wave problems," Zh. Prikl. Mekh. Tekh. Fiz., No. 2 (1973).
3. G. M. Lyakhov, Fundamentals of the Dynamics of Detonation Waves in Soils and Rock [in Russian], Nedra, Moscow (1974).
4. S. S. Grigoryan, "Fundamental concepts of soil dynamics," Prikl. Mat. Mekh., 24, No. 6 (1960).
5. G. M. Lyakhov and V. N. Okhitin, "Spherical detonation waves in multicomponent media," Zh. Prikl. Mekh. Tekh. Fiz., No. 2 (1974).
6. G. M. Lyakhov and V. N. Okhitin, "Plane waves in nonlinear viscous multicomponent media," Zh. Prikl. Mekh. Tekh. Fiz., No. 2 (1977).
7. S. K. Godunov and N. S. Kozin, "Structure of shock waves in a viscoelastic medium with a nonlinear dependence of the Maxwell viscosity on the material parameters," Zh. Prikl. Mekh. Tekh. Fiz., No. 5 (1974).
8. G. D. Babe, É. A. Bondareva, M. A. Kanibel'skii, and N. V. Shevchenko, "Spherical detonation in a viscoplastic medium," Izv. Akad. Nauk SSSR, Mekh. Tverd. Tela, No. 4 (1975).
9. É. A. Koshelev, "Evolution of the blast chamber formed by an underground explosion in soft soil," Zh. Prikl. Mekh. Tekh. Fiz., No. 2 (1975).
10. A. N. Zubkova and G. V. Rykov, "Propagation of one-dimensional stress waves in a viscoplastic medium," in: Proceedings of the Fifth All-Union Symposium on Propagation of Elastic and Elastoplastic Waves [in Russian], Nauka, Alma-Ata (1973).
11. E. C. Ting, "Wave propagations in a viscoelastic rod with temperature-dependent properties," J. Acoust. Soc. Am., 58, No. 2 (1975).
12. K. Akoi and M. Hori, "Consideration on wave propagation characteristics through soils as viscoelastic materials," in: Proceedings of the Sixteenth Japanese Congress on Materials Research, Kyoto (1973).
13. R. N. Jong, J. C. Dutertre, and R. J. Krizek, "Stress propagation in frequency-dependent clay soil," Trans. Soc. Rheol., 18, No. 3 (1974).

14. M. P. Zabinski and A. Phillips, "Spherical wave propagation in a viscoplastic medium — the case of unloading," Acta Mech., 20, Nos. 3-4 (1974).
15. N. E. Hoskin, "Method of characteristics for the solution of one-dimensional nonsteady flow equations," in: Computational Methods in Fluid Dynamics [Russian translation], Mir, Moscow (1967).
16. G. M. Lyakhov and K. S. Sultanov, "Similarity dispersion problems for waves in viscoplastic media," Zh. Prikl. Mekh. Tekh. Fiz., No. 6 (1975).

RELATION BETWEEN STATIC MECHANICAL CHARACTERISTICS AND IMPULSE STRESS IN METAL RODS

V. M. Glazkov, L. A. Kudryavtseva, and V. I. Sukhin

UDC 624.042.8:546.3.004.12

The basic difficulty in creating methods of calculation for the dynamic strength of systems and structures is the fact that the mechanical properties of the materials to be used in the construction have been insufficiently studied for dynamic loading. Existing papers [1-6] most frequently specify the value of the yield stress σ_s^{dyn}, i.e., the stress where irreversible plastic deformations begin to occur. However, the dynamic yield stress depends on the state of the material and on its static mechanical characteristics. For the purposes of investigation we took different materials as they were supplied and with different heat treatments (see Table 1).

The static mechanical characteristics were determined on a Gargarin press and an R-10 tension device in which the extension diagram was recorded.

The dynamic yield stress was determined by means of wire resistance strain gauges with a base length of 10 mm and a resistance of 100 Ω attached to the cylindrical rods (of length 150 mm and diameter 10 mm) at a distance of 120 mm from the impact end. The rod was set freely at a distance of 40 mm from the end of the shaft guides and centered accurately. The load was applied by means of a steel cylinder of length 10 mm and diameter 10 mm which was propelled with a velocity of the order of 500 m/sec. The sensor on the rod under investigation was included in an ordinary bridge circuit. The impulse corresponding to the dynamic yield stress, transmitted by the rod as a result of the blow of the cylinder-missile was recorded by means of an OK-17 M oscillograph. A more detailed account of the method and the calculation of the dynamic yield stress are given in [3].

Data determined for the mechanical characteristics ($\sigma_{0.2}$ is the yield stress, σ_c is the tensile strength, S_k is the true tensile strength) and for the dynamic yield stress σ_s^{dyn} are given in Table 1.

TABLE 1

Material	$\sigma_{0,2}$	σ_c	S_k	σ_s^{dyn}	$\sigma_s^{dyn}/\sigma_{0,2}$
	kg/mm²				0,2
Aluminum (annealed at 300°C)	4,3	8,4	31,2	18	4,2
Copper (annealed at 500°C)	7,1	22,4	76,3	32	4,5
" (as supplied)	9,2	23,7	69,4	30	3,3
Nickel (annealed at 800°C)	11,5	45	215	43	3,8
Nickel (as supplied)	—	47	208	55	—
Alloy D1 (as supplied)	15,5	23,2	36,7	23	1,5
Br. A7 (as supplied)	20,3	48	122,6	51	2,5
110G13BL (impact hardened)	86	112	125	93	1,1
St. 3 (annealed at 700°C)	20,9	40,6	96	80	3,83
Steel 45 (annealed at 700°C)	35,5	65,4	113,1	62	1,75
Steel 45 (as supplied)	41,2	74,8	117,3	82	1,99
4Kh13 (hardened + annealed at 500°C)	102	127,8	160,4	109	1,07
ShKh15 (as supplied)	44,4	71,7	131	55	1,2
ShKh15 (hardened + annealed) HR_C 35-40	163	171,7	220,2	161	0,99
ShKh15 (hardened + annealed) HR_C 45-50	174	183,5	225,4	170	0,98
ShKh15 (hardened) HR_C 60-62	195,5	211,1	224,5	194	0,99

Tomsk. Translated from Zhurnal Prikladnoi Mekhaniki i Tekhnicheskoi Fiziki, No. 5, pp. 135-137, September-October, 1977. Original article submitted September 27, 1976.

 0021-8944/77/1805-0700$07.50